RESEARCH ARTICLE

Anisotropic Gold Nanoparticles Synthesized using *Litchi chinensis* Leaf Extract and their Effect on Breast Cancer

Ramanjeet Kaur[1], Jitender Singh[2], Pramod K Avti[2], Vivek Kumar[3], Rajesh Kumar[1*]

[1]*Department of Physics, Panjab University, Chandigarh, India.*
[2]*Department of Biophysics, Post Graduate Institute of Medical Education and Research, Chandigarh, India.*
[3]*Centre for Medical Physics, Panjab University, Chandigarh, India.*

Received: 05th August, 2022; Revised: 03rd September, 2022; Accepted: 21st September, 2023; Available Online: 25th December, 2023

ABSTRACT

For its medicinal potential, especially in cancer therapy, eco-friendly gold nanoparticles (GNPs) have gained a lot of interest. This investigation used *Litchi chinensis* leaf extract (LLE) as a reducing agent for the one-step synthesis of regulated-size GNPs. Fourier transform infrared (FTIR) spectrum shows that the bio-molecules act as capping and reducing agents. The formation of GNPs has been confirmed using UV-vis absorption spectra. Effect of various synthesized parameters, i.e., reaction time (5–120 minutes), temperature (25–100°C), solvent quantity (5–45 µL), metal ion concentration (0.25–2 mM) and pH (2–10) has been studied. The size, distribution, and morphology (anisotropic) have been studied using field emission scanning electron microscopy (FESEM) and dynamic light scattering (DLS) techniques in the range of 10 to 70 nm. X-Ray diffraction (XRD) reveals that the particles were crystalline and had face-centered cubic (FCC) structure, and transmission electron microscopy (TEM) images revealed anisotropic morphology (spherical, hexagonal, and triangular). *In-vitro* studies of GNPs on breast cancer cell lines show cytotoxicity with cellular structural alterations and caused DNA damage without the micronuclei formation.

Keywords: Anisotropic, Cancer therapeutics, *Litchi chinensis* leaf extract, Gold nanoparticles.

International Journal of Drug Delivery Technology (2023); DOI: 10.25258/ijddt.13.4.01

How to cite this article: Kaur R, Singh J, Avti PK, Kumar V, Kumar R. Anisotropic Gold Nanoparticles Synthesized using *Litchi chinensis* Leaf Extract and their Effect on Breast Cancer. International Journal of Drug Delivery Technology. 2023;13(4):1131-1138.

Source of support: Nil.

Conflict of interest: None

INTRODUCTION

Nanotechnology is a versatile platform in the realm of contemporary materials science. Nanoparticles offer unique and unrivaled properties due to their size, shape, particle distribution, and prospective applications in biotechnology and health sciences.[1,2] Nanometer-sized materials have unique electrical, magnetic, and optical properties, allowing for a wide, versatile role in biological applications.[3-5] Gold nanoparticles (GNPs) are essential nanoscale materials that have been intensively explored because they have entirely new and better properties than bulk metals. Due to its exceptional size-dependent optoelectrical properties, novel technologies are involved in creating nanoparticles of noble metals, such as gold, that have acquired prominence.[6] GNPs, in particular, have proven to be a highly flexible deep-tissue imaging agent for various detection and imaging applications and are widely used in clinical settings.[7,8] Green chemistry and other biological processes are becoming increasingly popular, which has aided in developing easy and environmentally acceptable methods for synthesizing nanomaterials. Different physical and chemical approaches have been used to synthesize metallic nanoparticles.[9-14] These approaches pose health and safety concerns and are expensive to be carried out. The emergence and use of green technology are due to hazardous chemicals employed in the reduction and stabilization of nanoparticles, such as sodium borohydride ($NaBH_4$), tri-sodium citrate ($Na_3C_6H_5O_7$) hydroxylamine, and tetrakis (hydroxymethyl) phosphonium chloride (THPC), which are known to have negative consequences in their application use.[15,16] Several studies have been published on the utilization of products from natural sources such as algae and different parts of plants in the production of GNPs.[17-19] Microorganisms such as bacteria, fungi, and yeast have also been used to recover hazardous metals by reducing metal ions.[17,20,21] Litchi leaf, as a tissue of the litchi plant, is known to have a rich source of phenolics, such as flavonoids and lignans, which have reducing properties.[22]

Cancer is an aberrant kind of tissue development in which cells divide uncontrollably and independently, resulting in a steady rise in the number of dividing cells.[23] It is a serious health concern that causes substantial morbidity and death, resulting in an increase in the need for anticancer

**Author for Correspondence: rajeshphysicspu@gmail.com*

therapy throughout the world. The discovery of medicines for aggressive, quickly proliferating tumors is challenging in the fight against cancer.[24] Cancer can be treated with chemotherapy; however, it has a low selectivity and is limited by dose-limiting toxicity. Identifying appropriate therapies and medications for treating diverse forms of cancer with minimum side effects is a difficult task.[25] For greater efficacy and less toxicity, traditional approaches combined with new technology, such as controlled release and targeted medication delivery, might be helpful.[26] Nanomaterials are expected to transform cancer detection and treatment.[27] Several researchers have looked at the cytotoxicity, genotoxicity, and anticancer activities of green synthesis GNPs *in-vitro*. Colloidal GNPs synthesized from *H. brasiliensis* had shown cytotoxicity and genotoxicity in cancer cells.[28,29] Thio-glucose GNPs showed more cytotoxicity than naked GNPs and irradiation treatment alone in ovarian cancer cell lines.[30]

A simple, quick, and single-pot aqueous biosynthesis of GNPs utilizing *Litchi chinensis* leaf extract has been reported as part of the ongoing quest to synthesize GNPs using a green technique. In this study, we investigate the effect of various physicochemical parameters to understand their role in the synthesis and further their effect on breast cancer cells. Because of their particular features to boost potential therapeutic efficacy, GNPs may offer significant promise for development as an anticancer agent among the numerous nanoparticles.

MATERIAL AND METHODS

Materials

We purchased sodium hydroxide (NaOH), hydrochloroauric acid ($HAuCl_4.3H_2O$), and hydrochloric acid (HCl) from M/S Sigma Chemicals. *Litchi chinensis* fresh leaves were gathered from the Panjab University botanical garden in Chandigarh, India. Alkaloids, flavonoids, phytochemicals (epicatechin ($C_{15}H_{14}O_6$), procyanidin A2 ($C_{30}H_{24}O_{12}$), and proanthocyanidin B2 ($C_{30}H_{26}O_{12}$), as well as terpenoids and steroids, are the main components of *L. chinensis*. Epicatechin has greater reducing and scavenging abilities than procyanidin A2 and proanthocyanidin B2. Epicatechin's hydroxyl group and antioxidant activity give it a higher reducing potential.

Preparation of Leaf Extract

L. chinensis leaves were rinsed and cleaned with 3 rounds of DI water to remove dust. Then, the leaves were sun-dried and later crushed into fine powder. The powder was boiled for 20 minutes in 50 mL of DI water, filtered using Whatman filter paper no. 1, and the product was stored at 4°C until further use.[31]

Characterization of Gold Nanoparticles

UV-visible spectroscopy

UV–vis spectral experiments were performed to record surface plasmon resonance (SPR) (LABINDIA UV-3000$^+$ spectrometer). It obtained absorption spectra at various metal ion concentrations, altering LLE amounts, temperature, and pH values. The development of spherical GNPs is indicated by the SPR peak at 536 nm.

X-ray diffraction

For the X-ray diffraction (XRD) analysis of GNPs, the film was deposited on clean glass slides by drop-wise casting and recorded using Cu Kα (0.15406 nm) radiation (X' Pert PRO X-Ray diffractometer).

Transmission electron microscopy

The ultrastructural analysis of synthesized GNPs is carried out using a transmission electron microscope (Hitachi H-7500, Japan) with a CCD camera. TEM was used to examine the particle size and shape.

Fourier transform infrared

Fourier transform infrared (FTIR*)* in attenuated total reflection mode was used to screen the samples for FTIR spectra with 4 cm^{-1} resolution for the spectral range of 400 to 4000 cm^{-1} (Bruker Tensor 27, Switzerland).

Energy dispersive spectroscopy

GNPs solution was drop cast on a carbon lacey grid, and elemental composition was determined using energy dispersive spectroscopy (EDS) equipment (Quanta 200 FEG SEM, Bruker Model no. 630, Switzerland).

Field emission scanning electron microscopy

Field emission scanning electron microscopy (FESEM) was used to evaluate the morphological characteristics and particle size of nanoparticles (Hitachi SU8010 SERIES, Japan).

Dynamic light scattering

Dynamic light scattering (DLS) analysis on the size distribution of GNPs was performed using Malvern Zetasizer (ZEN3600).

Cytotoxicity Studies

Cell culture

Breast cancer MCF-7 cells were maintained in continuous culture of Eagles MEM in a humidified atmosphere of 5% CO_2 + 10% FBS and maintained at 37°C. After every 48 hours, the media was replaced with a fresh medium. The confluent monolayer of MCF-7 cells was detached using trypsin (0.25%) – EDTA (0.02% in PBS) by spinning at 200 x g for 2 minutes, followed by washing with a serum-free medium. The washed pellet was resuspended in 5 mL of complete media Eagle's MEM in a T25 flask and incubated at 37°C and 5% CO_2 for further processing.

Cytotoxicity

After the regular culturing of cells, approximately 1×10^4 cells were plated into 96 well plates and cultured overnight in a CO_2 incubator under humidified conditions. The next day, cells were treated with various concentrations of GNPs for different time durations. After the respective treatment time interval, cells were treated with MTT and incubated for 4 hours in the CO_2 incubator. The formed formazan crystals were dissolved in DMSO and read at a wavelength of 570 nm using a plate reader for cytotoxicity assessment.

Structural changes by microscopy

After studying the metallic nanoparticles-induced structural changes, the cells were visualized for their morphology under the phase contrast microscope after treating the cells with various concentrations and for different time intervals.

Apoptotic activity

Fluorescence microscopy was performed to assess the GNPs-induced apoptotic activity. After the cells were treated with GNPs, ethidium bromide, and acridine orange were used to stain the cells to evaluate the extent of DNA damage and micronuclei formation.

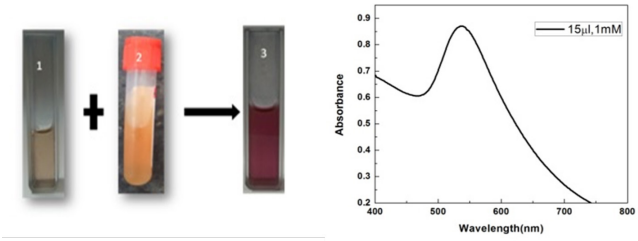

Figure 1: Visual confirmation for reduction of gold solution (1 mM, 6 mL) to GNPs using LLE (15 µL) and surface plasmon resonance of GNPs

RESULTS AND DISCUSSION

Preparation of Gold nanoparticles (GNPs) and UV- Vis Spectral Analysis

The $HAuCl_4.3H_2O$ (6 mL, 1-mM) solution was put on a stirrer. The 15 µL of LLE solution was added gradually to $HAuCl_4.3H_2O$ (1 mM) solution. Within a short duration, the color of the solution turns red wine, signifying the development of GNPs. GNPs are well known for their reddish hue in water, which is caused by the activation of surface plasmon vibrations in GNPs. Vial 1 contains $HAuCl_4.3H_2O$ solutions (1 mM), vial 2 contains the LLE, and the alteration in color of $HAuCl_4.3H_2O$ solution is reduced by LLE, indicating the formation of GNPs shown in vial 3. The existence of an SPR at 536 nm (Figure 1) revealed that the solution's different color was caused by GNPs (vial 3) surface plasmon vibrations. Most noble metals like gold and silver are considered free-electron systems. When the electromagnetic wave interacts, the conduction electrons oscillate under the electric field at the resonant frequency. The collective oscillation of conduction electrons is termed as Plasmon.[32] The alteration in color and an SPR peak at 536 nm indicates the reduction of the $HAuCl_4.3H_2O$ solution by LLE and its formation of GNPs.

Influence of Various Reaction Conditions

The influence of leaf extract quantity (µL) on the GNP production was investigated in this study by varying the LLE in the range 5 to 45 µL of $HAuCl_4.3H_2O$ (1 mM, 6 mL). It was observed that at 5 µL LLE, no SPR peak was obtained, as the LLE quantity was insufficient to reduce the gold salt solution to GNPs. Further, as the amount of LLE increased to 15 µL, the SPR peak was at 536 nm. At 30 and 45 µL LLE quantities, the SPR shifts towards higher wavelength, 538 and 540 nm, respectively, indicating the formation of GNPs in a concentration-dependent manner. As the concentration, the Lsize of GNPs also increases, leading to a shift in the SPR peak (Figure 2(a)). In 15 µL was the optimal value of LLE considered for further experiments based on the narrow distribution size and SPR peak position.[33]

The influence of gold salt solution concentration (0.25–2 mM) on the development of GNPs was also investigated (Figure 2(b)). The seed generation of gold results in the nanoparticle synthesis at 0.5 mM and above of gold salt concentration, as shown by the SPR peaks in Figure 2(b). The gold concentration of less than 0.5 mM is too small to generate the gold seed for GNP formation.[33] SPR peak was broad at lower concentrations of metal ions. $HuCl_4.3H_2O$ solution concentration of 1 mM showed the SPR peak at 536 nm, and further increasing in metal ion concentration to 2 mM shifted the SPR peak to 540 nm. This red shift in SPR indicates larger GNP formation as the $HuCl_4.3H_2O$ concentration rises.[23]

The variation of temperature was studied in the synthesis of GNPs. The experiments were conducted in the temperature range between 25 to 100°C. The reduction process was completed within 30 minutes at lower temperatures of 25°C, and the color of the solution transformed to red wine with an SPR peak at 536 nm. As the temperature increased to 40°C, the SPR peak shifted to a higher wavelength around 538 nm, as shown in Figure 2(c). At a temperature of 60 to 100°C, the reaction was too fast; as LLE was added to the gold salt solution, the color of the solution immediately altered to red wine. The reaction was completed in a few seconds with less SPR peak intensity.

The influence of reaction time on the production of GNPs is also studied. The intensity of the SPR peak at 536 nm was increased with reaction time, as shown in Figure 2(d). The $HAuCl_4.3H_2O$ reacts with LLE, and GNPs begin to develop within 10 minutes. The SPR spectra reveal the variations in peak intensity. The reaction takes 30 minutes to complete; after that point, prolonging the reaction doesn't further affect the development of nanoparticles, evidenced by unchanged SPR peaks at 536 nm. The color of the $HAuCl_4.3H_2O$ solution changes to red at different time intervals between 0 to 120 minutes (Figure 2(e)).

Effect of pH on GNP Stability

The influence of pH values on the stability of GNPs was discovered as most of the nanoparticles were utilized in biological *in-vitro* and *in-vitro* experiments. The GNPs found to be stable in a wide range of pH 3 to 8 are observed to have no Bathochromic shift or hypsochromic shift in the SPR peaks. It was observed from UV-vis spectroscopy that the SPR peak remains at 536 nm for the pH range 2 to 10 used. The broader absorption at lower pH 2 and 10 could be attributed to the nanoparticles changing size (Figure 3).[34] The GNP's stability could be attributed to the presence of surface stabilizing agents present in LLE.

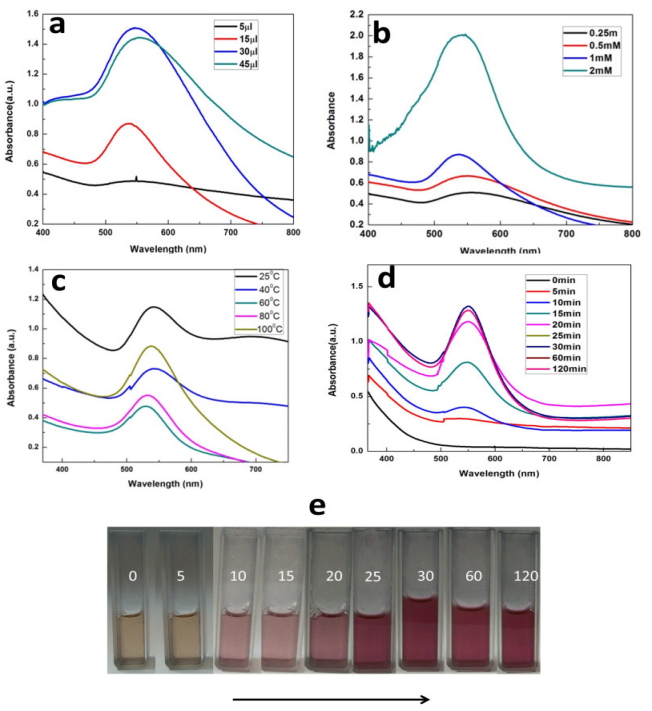

Figure 2: UV–vis absorption spectra of GNPs (a) varying LLE quantity, (b) metal ion concentration, (c) temperature, (d) duration of reaction, and (e) visual confirmation from the color change of the solution.

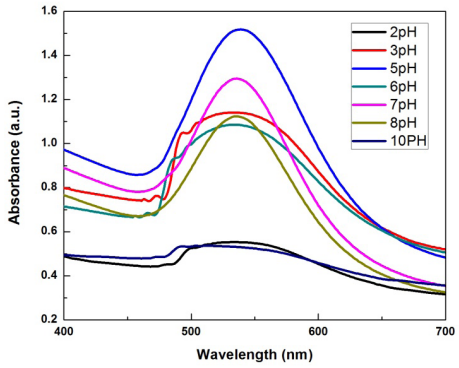

Figure 3: UV–vis absorption spectra of $HAuCl_4.3H_2O$ (1 mM) solution with LLE (15 µL) at 25°C at various pH values.

Fourier Transform Infrared

The chemical components involved in converting $HAuCl_4.3H_2O$ (1 mM) to GNPs by LLE were identified using FTIR analysis shown in Figure 4. According to FTIR analysis, the leaf extract contains flavonoids, phenol, hydroxyl, and amide, which function as reducing and stabilizing agents.[35] The band 2153.03 to 2147.63 cm^{-1} shifts due to aromatic C-H stretching, 1732.10 cm^{-1} band due to C=O aliphatic ketone. The band shift from 1391.10 to 1407.53 cm^{-1} corresponds to aldehyde (C-H) bending due to the aromatic ring, 1099.15 to 1060.14 $cm^{-1,}$ the C-N stretching vibration of polyphenols. Table 1 represents the functional groups of LLE and GNPs corresponding to the respective frequency. The constituents present in LLE were responsible for reducing gold salt solution

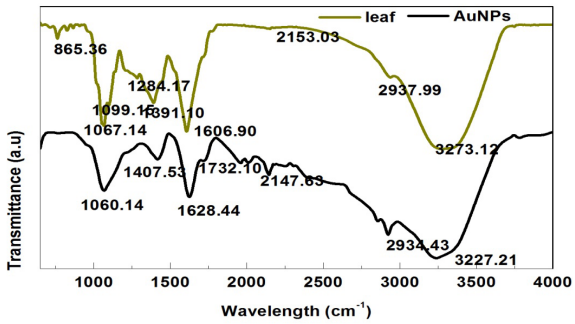

Figure 4: FTIR spectra of GNPs mediated by LLE(15 µL) (black line) and LLE (black line) at 25°C, $HAuCl_4.3H_2O$ (1 mM) solution.

to GNPs. The presence of epicatechin ($C_{15}H_{14}O_6$), procyanidin A2 ($C_{30}H_{24}O_{12}$), and proanthocyanidin B2 ($C_{30}H_{26}O_{12}$) in LLE adsorbed on the surface of GNPs due to which GNPs were stable for long time.[36] The reaction process between the Au^{3+} ion and epicatechin (polyphenol form) produces an intermediate product called Au-epicatechin, which is then oxidized to produce quinone, a hydrogen atom, and electrons (Figure 5). The electrons converted the Au^{3+} ion into the atom Au^0.

Dynamic Size Determination

DLS measures the variations in scattered light intensity brought on by particle mobility. Particle size distribution analysis by DLS is shown in Figure 6. GNPs were discovered to have an average hydrodynamic size of about 70 nm.

Ultrastructural determination

Biosynthesized GNP has been identified as crystalline using XRD analysis. GNPs XRD pattern is displayed in Figure 7(a). The sharp peaks corresponding to Bragg's reflections (111), (200), (220), and (311) sets of lattice planes were based on the FCC structure with 2θ values (38.25°, 44.29°, 64.51°, and 77.49°).[41,42] Bragg's reflections agreed with JCPDS file no: 04–0784, suggesting their purity of crystalline gold for the synthesized GNPs.[41] The average crystalline size was calculated using the Debey Scherer formula:[43]

$$D = \frac{0.9\lambda}{\beta cos\theta}$$

Where denotes X-ray wavelength, refers to full-width half maxima, is the angle in radians, and D is crystalline size calculated for the dominant (111) plane and found to be around 14 nm.

FESEM reveals the surface morphology and particle size distribution of biosynthesized nanoparticles. The majority of the biosynthesized GNPs were found to be spherical and irregular in shape. The FESEM results are shown in Figure 7(b), and nanoparticle size was found in the range of 20 to 70 nm. The average particle size was 45 nm.

The EDS spectrum validated the nature, purity, and elemental composition of the produced biogenic GNPs. The EDS profile displays a significant gold signal and faint carbon and oxygen peaks (Figure 7(c)), which could have come

Table 1: FTIR of LLE and GNPs bands

GNPs frequency range (cm^{-1})	*LLE frequency range (cm^{-1})*	*Functional groups*	*References*
-	1067	C-O stretching	37
3227.21	3273.12	O-H stretching of phenol	38
2934.43	2937.99	secondary amines	39
2147.63	2153.03	Aromatic C-H stretching	23
1628.44	1606.90	amide I and III bands - proteins	39
1407.53	1391.10	-OH bending of carboxylic acid	40
1060.14	1099.15	C-N stretching of polyphenols	40

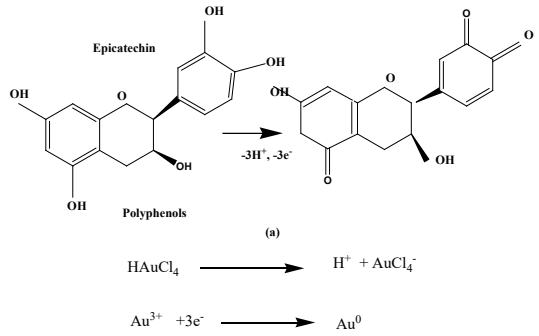

Figure 5: The reaction mechanism of $HAuCl_4$ to GNPs

from biomolecules bonded to the GNP surface and acting as stabilizing agents.[44] Nanoparticles produced from LLE are coated by a thin layer of organic material present in LLE that keeps them stable in solution.

TEM images disclose the shape and size of GNPs. Figure 7(d) shows the TEM image of GNPs. TEM reveals the particles were mainly spherical, with few triangle and hexagonal shapes, and their size was found to be 10 to 60 nm. Bio-capping agents are supposed to manage the size and morphology of nanoparticles during the bio-reduction reaction. They may bind to GNPs on the nanoparticle's surface, resulting in an anisotropic morphology.[45] The average particle size is of the order of 45 nm.

Cytotoxicity Assays

Figure 8 shows the effect of GNPs on breast cancer MCF-7 cells at various doses and duration. MTT results show no effect on cell viability treated up to 20 µL of GNPs for 24 hours. However, 40 µL of GNPs reduced the cell viability to approximately 20% at 24 hours, respectively. The dose of 40 µL of GNPs reduced cell viability to 20 and 30% at 24 and 48 hours, respectively. This clearly shows that the anisotropic GNPs reduced the cell viability at higher doses and time periods. Similar reports were observed in the cervical cancer cells using the green GNPs synthesis using *Benincasa hispidia*,[46] wherein the maximum cytotoxicity was observed at 48h treated with 10 µg/mL. GNPs synthesized using *Mimosa*

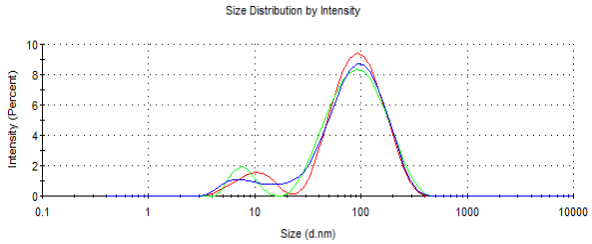

Figure 6: The size distribution intensity of GNPs was recorded at 25°C, LLE (15 µL), and $HAuCl_4.3H_2O$ (1 mM) solution

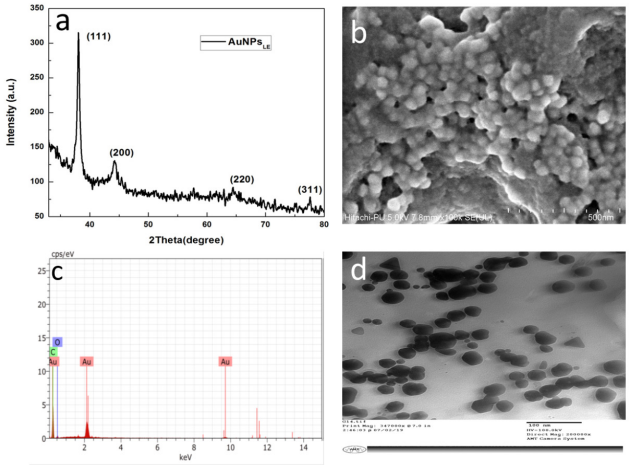

Figure 7: GNPs recorded (a) XRD, (b) SEM, (c) EDS, and (d) TEM at 25°C, LLE(15 µL) and $HAuCl_4.3H_2O$ (1mM) solution

tenuiflora had a cytotoxic effect on the endothelial cells.[47] Similarly, the structural changes were recorded by acquiring the optical images before and after treatment with GNPs (Figure 8 B). The images clearly show that GNPs altered the cellular structures to a greater extent at the doses of 20 and 40 µL at 48 hours (Figure 8 B) as compared to 24 hours (images not shown). The observable structural changes include the cellular shape, cell aggregation, cytoplasm condensation, and decreased cell number after treatment as compared to the untreated cells, *Benincasa hispidia*-mediated synthesized GNPs also showed some of the cellular structural changes, as noted in the present study.[46] Further, fluorescence microscopy performed micronuclei assessment and DNA damage analysis using acridine orange and ethidium bromide fluorescent dyes (Figure 8C). It is clear from the study that there was no micronuclei formation at the doses used and for up to 48 hours, as evidenced by green fluorescence as seen in the control cells (Figure 8 C, control), which otherwise would change to orange with the formation of micronuclei (hence images not included). However, there was damage to the nuclear DNA at 20 and 40 µL at 48 hours (Figure 8C, GNPs (20) and GNP (40)) as compared to 24 hours (images not included). It is known that micronuclei are extranuclear entities that are not included in the nucleus after cell division. Ethidium bromide is the DNA-binding dye that enters the cells after membrane damage. From the results of MTT and structural changes observed from the optical images, it can be assumed that the GNPs have a

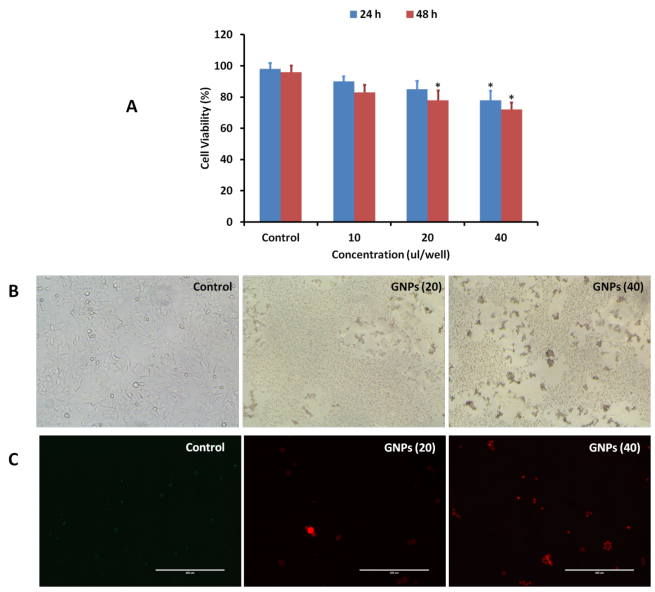

Figure 8: Cytotoxicity studies of GNPs on breast cancer cells (MCF-7). (A) Cell viability analysis using MTT assay, (B) structural changes using optical microscopy at 48 hours, (C) Acridine orange and ethidium bromide staining for micronuclei and DNA damage at 48 hours.

cytotoxic effect and bind to DNA to cause cellular damage. Similar results were also observed in a recent study, where the mechanism accounted for ROS formation generation due to GNP treatment.[46] It is also known that the ROS generation causes the DNA damage. So it can be assumed that the GNPs had no effect in micronuclei formation, which is usually seen during the cancer initiation and progression. However, GNPs had damaged the MCF-7 breast cancer cells which is seen with the red fluorescence of ethidium bromide dye binding to the DNA [Figure 8C, GNP(20) and GNP(40)]. These results clearly show that GNPs at higher doses and at long duration can damage the breast cancer cells.

CONCLUSION

The prospective uses of biosynthesized nanoparticles as novel advanced nanomaterials are now being researched in regard to nanoparticle synthesis employing biological components. A simple one-step method to produce GNPs using LLE acts as both a reducing and capping agent. LLE has phytochemical constituents epicatechin ($C_{15}H_{14}O_6$), procyanidin A2 ($C_{30}H_{24}O_{12}$), and proanthocyanidin B2 ($C_{30}H_{26}O_{12}$). The phytochemical helps to reduce gold ions to GNPs. The stability of GNPs was studied using a variety of physicochemical criteria. Various amounts of leaf extract, varying temperatures, and metal ion concentrations were all evaluated to reach the optimal size. When leaf extract comes into contact with gold salt solution, the formation of GNPs begins with the seed generation process. The 15 µL LLE treated at 25°C temperature for 20 minutes resulted in more than 90% of $HAuCl_4.3H_2O$ (1 mM) forming GNPs. Further, the stability of GNPs was found to be most stable in the pH range of 3 to 8, as deduced from the SPR peaks. Biomolecules present in the LLE might be accountable for the reduction and capping of GNPs, as evidenced by FTIR studies. XRD examination revealed that the GNPs have an FCC crystalline phase of 14 nm. The morphology of the synthesized GNPs was mostly spherical, with a few triangular and hexagonal forms. The average size of produced GNPs, as evidenced by TEM, was around 45 nm. FESEM studies also reveal the average size of GNPs to be approximately 45 nm. The quality of the produced GNPs validated by EDS spectrum spectroscopy confirms that the nanoparticles produced are from gold. DLS reveals the hydrodynamic size of 70 nm. This green synthetic approach produced both cost-effective and simple nanoparticles, stable in the solution for a longer duration and retained their definite shape and size. These synthesized GNPs also show the ability to damage the breast cancer cells, as studied by MTT, affecting the mitochondrial enzyme's cellular structural alterations and causing DNA damage. Such nanoparticles will have long-lasting and varied biomedical applications in the future, considering the inexpensive, non-hazardous, and uncomplicated methods used for their synthesis.

ACKNOWLEDGMENT

The SAIF and CIL Department, Panjab University, Chandigarh, supported TEM and FESEM analysis.

REFERENCES

1. Magnusson MH, Deppert K, Malm JO, Bovin JO, Samuelson L. Gold nanoparticles: Production, reshaping, and thermal charging. Journal Nanoparticle Research 1999;1(2):243–51. https://doi.org/10.1023/A:1010012802415
2. Santhoshkumar J, Rajeshkumar S, Venkat Kumar S. Phyto-assisted synthesis, characterization and applications of gold nanoparticles – A review. Biochemistry and Biophysics Reports. 2017;11: 46–57. https://doi.org/10.1016/j.bbrep.2017.06.004
3. Shankar SS, Deka S. Metal nanocrystals and their applications in biomedical systems. Advance Material. 2011;3(2):169–95. https://doi.org/10.1166/sam.2011.1150
4. Gao Y, Wu Y, Di J. Colorimetric detection of glucose based on gold nanoparticles coupled with silver nanoparticles. Spectrochimica Acta - Part A: Molecular and Biomolecular Spectroscopy. 2017;173:207–12. https://doi.org/10.1016/j.saa.2016.09.023.
5. Shan W, Pan Y, Fang H, Guo M, Nie Z, Huang Y. An aptamer-based quartz crystal microbalance biosensor for sensitive and selective detection of leukemia cells using silver-enhanced gold nanoparticle label. Talanta. 2014;126:130–5. https://doi.org/10.1016/j.talanta.2014.03.056
6. Levitas VI, Samani K. Size and mechanics effects in surface-induced melting of nanoparticles. Nature Communication. 2011;2(1). https://doi.org/10.1038/ncomms1275.
7. Aitken RJ, Chaudhry MQ, Boxall ABA, Hull M. Manufacture and use of nanomaterials: Current status in the UK and global trends. Occupational Medicine. 2006;56: 300–6. https://doi.org/10.1093/occmed/kql051.
8. He H, Xie C, Ren J. Nonbleaching fluorescence of gold nanoparticles and its applications in cancer cell imaging. Analytical Chemistry. 2008;80(15):5951–7. https://doi.org/10.1021/ac8005796.
9. Naik RR, Stringer SJ, Agarwal G, Jones SE, Stone MO.

Biomimetic synthesis and patterning of silver nanoparticles. Nature Materials. 2002;1(3):169–72. https://doi.org/10.1038/nmat758.

10. Ng VWK, Avti PK, Bédard M, Lam T, Rouleau L, Tardif JC, et al. Miktoarm star conjugated multifunctional gold nanoshells: Synthesis and an evaluation of biocompatibility and cellular uptake. Journal of Material Chemistry B. 2014;2(37):6334–44. https://doi.org/10.1039/c4tb00722k.
11. Mafuné F, Kohno JY, Takeda Y, Kondow T. Full physical preparation of size-selected gold nanoparticles in solution: Laser ablation and laser-induced size control. Journal of Physical Chemistry B. 2002;106(31):7575–7. https://doi.org/10.1021/jp020577y
12. Sau TK, Pal A, Jana NR, Wang ZL, Pal T. Size controlled synthesis of gold nanoparticles using photochemically prepared seed particles. Journal of Nanoparticle Research. 2001;3(4):257–61. https://doi.org/10.1023/A:1017567225071.
13. Okitsu K, Yue A, Tanabe S, Matsumoto H, Yobiko Y. Formation of colloidal gold nanoparticles in an ultrasonic field: Control of rate of gold(III) reduction and size of formed gold particles. Langmuire. 2001;17(25):7717–20. https://doi.org/10.1021/la010414l.
14. Nadeau JL. Synthesis of Gold Nanoparticles /. Introd to Exp Biophys - A Lab Guid. 2020;154–9. https://doi.org/10.1201/b18283-20.
15. Tang B, Sun L, Li J, Zhang M, Wang X. Sunlight-driven synthesis of anisotropic silver nanoparticles. Chemical Engineering Journal. 2015;260:99–106. https://doi.org/10.1016/j.cej.2014.08.044.
16. Bhattacharya D, Saha B, Mukherjee A, Ranjan Santra C, Karmakar P. Gold Nanoparticles Conjugated Antibiotics: Stability and Functional Evaluation. Nanoscience Nanotechnology. 2012;2(2):14–21. https://doi.org/10.5923/j.nn.20120202.04.
17. Sastry M, Ahmad A, Khan MI, Kumar R. Microbial Nanoparticle Production. In: Nanobiotechnology. 2005: 126–35. https://doi.org/10.1002/3527602453.ch9.
18. Dubey SP, Lahtinen M, Sillanpää M. Tansy fruit mediated greener synthesis of silver and gold nanoparticles. Process Biochemistry. 2010;45(7):1065–71. https://doi.org/10.1016/j.procbio.2010.03.024.
19. Esumi K, Kameo A, Suzuki A, Torigoe K, Yoshimura T, Koide Y, et al. Preparation of gold nanoparticles using 2-vinylpyridine telomers possessing multi-hydrocarbon chains as stabilizer. Colloids Surfaces A Physicochem Engineering Aspects. 2001;176(2–3):233–7. https://doi.org/10.1016/S0927-7757(00)00592-6.
20. Dhanasekar NN, Rahul GR, Narayanan KB, Raman G, Sakthivel N. Green chemistry approach for the synthesis of gold nanoparticles using the fungus Alternaria sp. Journal of Microbiology Biotechnology. 2015;25(7):1129–35. https://doi.org/10.4014/jmb.1410.10036
21. Sinha S, Pan I, Chanda P, Sen SK. Nanoparticles fabrication using ambient biological resources. Journal of Applied Bioscience. 2009;19:1113–30.
22. Ibrahim SRM, Mohamed GA. Litchi chinensis: Medicinal uses, phytochemistry, and pharmacology. Journal of Ethnopharmacology. 2015; 174: 492–513. https://doi.org/10.1016/j.jep.2015.08.054.
23. Dubey SP, Lahtinen M, Sillanpää M. Green synthesis and characterizations of silver and gold nanoparticles using leaf extract of Rosa rugosa. Colloids Surfaces A Physicochemistry Engineering Aspects. 2010;364(1–3):34–41. https://doi.org/10.1016/j.colsurfa.2010.04.023.
24. Lahir YH, Avti P. Nanomaterials and Their Interactive Behavior with Biomolecules, Cells and Tissues. Nanomaterials and Their Interactive Behavior with Biomolecules, Cells and Tissues. 2020. https://doi.org/10.2174/9789811461781120010l
25. Bédard M, Avti PK, Lam T, Rouleau L, Tardif JC, Rhéaume É, et al. Conjugation of multivalent ligands to gold nanoshells and designing a dual modality imaging probe. Journal Material Chemistry B. 2015;3(9):1788–800. https://doi.org/10.1039/c4tb01811g.
26. Chauhan A, Ranjan R, Avti P, Gulbake A. Tailoring the nanoparticles surface for efficient cancer therapeutics delivery. International Journal of Applied Pharmaceutics. 2020;12(Special Issue 4):11–7. https://doi.org/10.22159/ijap.2020.v12s4.40099.
27. Rosarin FS, Arulmozhi V, Nagarajan S, Mirunalini S. Antiproliferative effect of silver nanoparticles synthesized using amla on Hep2 cell line. Asian Pacific Journal of Tropical Medicine. 2013;6(1):1–10. https://doi.org/10.1016/S1995-7645(12)60193-X.
28. Santos NM, Gomes AS, Cavalcante DGSM, Santos LF, Teixeira SR, Cabrera FC, et al. Green synthesis of colloidal gold nanoparticles using latex from Hevea brasiliensis and evaluation of their *in vitro* cytotoxicity and genotoxicity. IET Nanobiotechnology. 2019;13(3):307–15. https://doi.org/10.1049/iet-nbt.2018.5225.
29. Song K, Xu P, Meng Y, Geng F, Li J, Li Z, et al. Smart gold nanoparticles enhance killing effect on cancer cells. International Journal of Oncology. 2013;42(2):597–608. https://doi.org/10.3892/ijo.2012.1721.
30. Geng F, Song K, Xing JZ, Yuan C, Yan S, Yang Q, et al. Thio-glucose bound gold nanoparticles enhance radio-cytotoxic targeting of ovarian cancer. Nanotechnology. 2011;22(28):285101. https://doi.org/10.1088/0957-4484/22/28/285101.
31. Kaur R, Avti P, Kumar V, Kumar R. Effect of various synthesis parameters on the stability of size controlled green synthesis of silver nanoparticles. Nano Express. 2021; 2(2): 020005. https://doi.org/10.1088/2632-959X/abf42a.
32. Moores A, Goettmann F. The plasmon band in noble metal nanoparticles: An introduction to theory and applications. New Journal of Chemistry. 2006; 30: 1121–32. https://doi.org/10.1039/b604038c.
33. Ghazy OA, Ibrahim MM, Abou Elfadl FI, Hosni HM, Shehata EM, Deghiedy NM, et al. PEDOT:PSS incorporated silver nanoparticles prepared by gamma radiation for the application in organic solar cells. Journal of Radiation Research Applied Science. 2015;8(2):166–72. https://doi.org/10.1016/j.jrras.2014.09.007.
34. Velmurugan P, Cho M, Lee SM, Park JH, Lee KJ, Myung H, et al. Phyto-crystallization of silver and gold by Erigeron annuus (L.) Pers flower extract and catalytic potential of synthesized and commercial nano silver immobilized on sodium alginate hydrogel. Journal of Saudi Chemical Society. 2016;20(3):313–20. https://doi.org/10.1016/j.jscs.2014.09.004.
35. Jyoti K, Baunthiyal M, Singh A. Characterization of silver nanoparticles synthesized using Urtica dioica Linn. leaves and their synergistic effects with antibiotics. Journal Radiation Research Applied Science. 2016;9(3):217–27. https://doi.org/10.1016/j.jrras.2015.10.002.

36. Sharma P, Babu PJ, Bora U. Sapindus mukorossi aqueous fruit extract as reducing, capping and dispersing agents in synthesis of gold nanoparticles. Micro Nano Letter. 2012;7(12):1296–9. https://doi.org/10.1049/mnl.2012.0684.
37. Xu X, Xie H, Hao J, Jiang Y, Wei X. Eudesmane sesquiterpene glucosides from lychee seed and their cytotoxic activity. Food Chemistry. 2010;123(4):1123–6. https://doi.org/10.1016/j.foodchem.2010.05.073.
38. Ahmad T, Irfan M, Bustam MA, Bhattacharjee S. Effect of Reaction Time on Green Synthesis of Gold Nanoparticles by Using Aqueous Extract of Elaise Guineensis (Oil Palm Leaves). Procedia Engineering. 2016: 467–72. https://doi.org/10.1016/j.proeng.2016.06.465.
39. Xin Lee K, Shameli K, Miyake M, Kuwano N, Bt Ahmad Khairudin NB, Bt Mohamad SE, et al. Green Synthesis of Gold Nanoparticles Using Aqueous Extract of Garcinia mangostana Fruit Peels. Journal of Nanomaterial. 2016;2016:1-7. https://doi.org/10.1155/2016/8489094.
40. Kumar I, Mondal M, Meyappan V, Sakthivel N. Green one-pot synthesis of gold nanoparticles using Sansevieria roxburghiana leaf extract for the catalytic degradation of toxic organic pollutants. Material Reseach Bulltein. 2019;117:18–27. https://doi.org/10.1016/j.materresbull.2019.04.029.
41. Ankamwar B, Salgaonkar M, Sur UK. Room temperature green synthesis of anisotropic gold nanoparticles using novel biological fruit extract. Inorganic Nano-Metal Chemisry. 2017;47(9):1359–63. https://doi.org/10.1080/24701556.2017.1284121.
42. Fazal S, Jayasree A, Sasidharan S, Koyakutty M, Nair S V., Menon D. Green synthesis of anisotropic gold nanoparticles for photothermal therapy of cancer. ACS Applied Material Interfaces. 2014;6(11):8080–9. https://doi.org/10.1021/am500302t.
43. Bindhu MR, Umadevi M. Silver and gold nanoparticles for sensor and antibacterial applications. Spectrochim Acta - Part A Mol Biomolecule Spectroscopy. 2014;128:37–45. https://doi.org/10.1016/j.saa.2014.02.119.
44. Shankar SS, Rai A, Ahmad A, Sastry M. Rapid synthesis of Au, Ag, and bimetallic Au core-Ag shell nanoparticles using Neem (Azadirachta indica) leaf broth. Journal of Colloid Interface Science. 2004;275(2):496–502. https://doi.org/10.1016/j.jcis.2004.03.003.
45. Fei X, Jia M, Du X, Yang Y, Zhang R, Shao Z, et al. Green synthesis of silk fibroin-silver nanoparticle composites with effective antibacterial and biofilm-disrupting properties. Biomacromolecules. 2013;14(12):4483–8. https://doi.org/10.1021/bm4014149.
46. Saqr A Al, Khafagy ES, Alalaiwe A, Aldawsari MF, Alshahrani SM, Anwer MK, et al. Synthesis of gold nanoparticles by using green machinery: Characterization and *in vitro* toxicity. Nanomaterials. 2021;11(3):1–14. https://doi.org/10.3390/nano11030808.
47. Rodríguez-León E, Rodríguez-Vázquez BE, Martínez-Higuera A, Rodríguez-Beas C, Larios-Rodríguez E, Navarro RE, et al. Synthesis of Gold Nanoparticles Using Mimosa tenuiflora Extract, Assessments of Cytotoxicity, Cellular Uptake, and Catalysis. Nanoscale Research Letter. 2019;14(1): 1-16. https://doi.org/10.1186/s11671-019-3158-9.